Biomaterials Science

ROYAL SOCIETY OF CHEMISTRY

PAPER

View Article Online
View Journal

Cite this: DOI: 10.1039/d0bm00843e

3D hydrogel mimics of the tumor microenvironment: the interplay among hyaluronic acid, stem cells and cancer cells†

Sara Amorim, *[a,b] Diana Soares da Costa, [a,b] Iva Pashkuleva, [a,b] Celso A. Reis,[c,d,e,f] Rui L. Reis [a,b] and Ricardo A. Pires *[a,b]

Received 21st May 2020,
Accepted 22nd October 2020

DOI: 10.1039/d0bm00843e

rsc.li/biomaterials-science

The present work reports on a 3D model of the tumor microenvironment that contains hyaluronic acid (HA) and alginate, and demonstrates the utility of this model to study the effect of HA size on the crosstalk between cancer cells and mesenchymal stem cells (MSCs). The system incorporates a core that contains HA of specific size (*i.e.* 6.4, 741 or 1500 kDa) with encapsulated epithelial MKN45 cancer cells and a shell with MSCs that mimic the presence of stem cells next to the tumor site. It was found that short HA (*i.e.* 6.4 kDa) promotes the invasion of cancer cells from the core to the shell, whereas longer HA (*i.e.* 741 and 1500 kDa) recruits the MSCs into the core, *i.e.* the tumor site, where a reduction of the formation of cancer cell aggregates was observed. In summary, the developed 3D model recapitulates some key tumor features related to the effect of HA size on both cancer cell invasiveness and MSC behavior at the tumor site.

Introduction

The interactions of cancer cells (CCs) with the components of the surrounding microenvironment, such as proteins, glycoproteins, proteoglycans, signaling molecules and different cell types, create a complex tumor microenvironment (TME).[1–3] Changes in the TME impact cancer progression: unbalanced synthesis and degradation of its components lead to altered stiffness, elasticity, permeability,[4] and biochemical composition.[5,6] One of the TME components that plays a critical role in cancer invasiveness is hyaluronic acid (HA).[7,8] The abnormal synthesis of HA by the synthases and the deregulated digestion by hyaluronidases lead to the accumulation of HA with different molecular weights (M_ws) in the basement membrane of cancer cells.[7] The accumulated HA can trigger various signaling pathways (*e.g. via* interaction with HA-specific transmembrane receptor CD44) that affect cell proliferation, migration or even latency and apoptosis.[6] The cell response is dependent on the M_w of HA:[9,10] low M_w HA (<100 kDa) is pro-inflammatory and promotes CC invasion and metastasis, while high M_w (>1000 kDa) HA induces CC latency.[7,11] The TME is also governed by the crosstalk between CCs and healthy cells from the surrounding microenvironment (*e.g.* mesenchymal stem cells – MSCs, macrophages and fibroblasts, among others).[12–14] MSCs are linked to tumor progression but their role is controversial. Some authors show that MSCs induce tumor growth by disrupting cell-to-cell contact and promoting CC invasion.[15] Other works suggest that MSCs inhibit the invasiveness of CCs by reducing their drug resistance.[16] In fact, the MSCs' activity depends on their density. It has been reported that a 1 : 1 MSC : CC ratio induces upregulation of metastatic genes; whereas a lower ratio (*e.g.* 1 : 2) results in tumor remission.[17–19] The presence of MSCs can also influence the CC aggregation: the MSCs added to pre-formed aggregates caused disorganization of the structures, while the MSCs present since the beginning of the formation of CC spheroids enhanced spatial organization and homogeneity.[20]

The complexity of the TME as well as the mismatch between different animal models and the human cellular environment impose the development of 3D models that mimic the biochemical and mechanical features of the TME as a valuable tool to study cancer progression and/or the efficiency of different treatments.[21,22] Herein, we developed a

[a]3B's Research Group, I3Bs – Research Institute on Biomaterials, Biodegradables and Biomimetics, University of Minho, Headquarters of the European Institute of Excellence on Tissue Engineering and Regenerative Medicine, AvePark, Parque de Ciência e Tecnologia, Zona Industrial da Gandra, 4805-017 Barco, Portugal. E-mail: sara.amorim@i3bs.uminho.pt, rpires@i3bs.uminho.pt
[b]ICVS/3B's - PT Government Associate Laboratory, Braga/Guimarães, Portugal
[c]i3S, University of Porto, Portugal
[d]IPATIMUP, Porto, Portugal
[e]Department of Pathology and Oncology, Faculty of Medicine, Porto University, Portugal
[f]Institute of Biomedical Sciences Abel Salazar, University of Porto, Portugal

†Electronic supplementary information (ESI) available. See DOI: 10.1039/d0bm00843e

3D co-culture system that recapitulates some important features of the TME: the core is the cancer site with encapsulated CCs exposed to HA of specific M_ws that are known to elicit different CC responses, *e.g.* migration or latency, and the surrounding shell contains healthy MSCs that can crosstalk with the CCs present at the cancer site (*i.e.* core of the hydrogel). We demonstrate that this system can replicate the key features of cancer progression and invasiveness.

Materials and methods

Materials

Sodium hyaluronates (HA) with M_ws of 6.4, 741 and 1500 kDa were acquired from Lifecore (USA) and sodium alginate (Alg, UP VLVG, >75 kDa) from Pronova (Norway). The CD44 monoclonal antibody (Ascites, AM06286SU-N) was purchased from ACRIS. The FITC-labelled CD90 (Thy-1) monoclonal antibody (eBio5E10 (5E10)) was obtained from eBioscience™. The other antibodies, rabbit monoclonal to Vimentin [EPR3776], rabbit monoclonal to E-cadherin [EP700Y] and rabbit monoclonal to alpha smooth muscle actin [E184], were obtained from Abcam. The secondary antibodies IRDye® 800CW Goat-anti-Rabbit and IRDye® 800CW Goat-anti-Mouse were obtained from LI-COR Biosciences.

Methods

Hyaluronic acid modification with FITC. Fluoresceinamine (FITC) was coupled to the carboxylic groups of HA of different M_ws (*i.e.* 6.4, 741 and 1500 kDa) using *N*-(3-dimethylaminopropyl)-*N*′-ethylcarbodiimide hydrochloride (EDC) chemistry as previously described.[23]

Preparation of hydrogels. Alg and HA were dissolved in Milli-Q water and NaCl 0.15 M, respectively. Both solutions were mixed to a final concentration of 20 mg mL^{-1} of Alg and 1 mg mL^{-1} of HA. Spheres (core of the 3D system) were extruded (27G syringe) into a $CaCl_2$ solution (100 mM) under constant magnetic stirring. After gelation, the spheres were washed with Tris-buffered saline (TBS) supplemented with 15 mM $CaCl_2$. The Alg or Alg-HAM_w spheres were embedded in a pre-gelated Alg disc and the core–shell hydrogels were allowed to crosslink on a QGel® mould immersed in 50 mM $CaCl_2$ for 15 min. The final construct was washed with TBS-$CaCl_2$.

Culture, expansion and seeding of a gastric cancer cell line and bone marrow mesenchymal stem cells. The human gastric cancer cell line MKN45 (passages 6 or 7) was cultured in RPMI-1640 medium (Sigma-Aldrich, Portugal) supplemented with 10% fetal bovine serum (FBS; Gibco) and 1% antibiotic/antimycotic solution (final concentration of penicillin: 100 units per mL, streptomycin: 100 mg mL^{-1} and 25 μg mL^{-1} amphotericin B; Gibco, UK). Human bone marrow aspirates were collected from patients subjected to total hip replacement surgery, under the scope of an agreement (Ref. DC 05/2015) with Hospital da Prelada (Porto, Portugal). Bone marrow mesenchymal stem cells (bmMSCs) were isolated from the tissue according to a previously published procedure.[24] Afterwards, bmMSCs were expanded in Minimum Essential Medium (MEM) alpha medium (αMEM; Sigma-Aldrich, Germany) supplemented with 1% antibiotic/antimycotic (Gibco) and 10% FBS and used at passage 3. Both cell types, MKN45 and bmMSCs, were cultured in a 5% CO_2 incubator maintained at 37 °C. For the encapsulation of cells into the hydrogel, MKN45 and bmMSCs were washed with PBS and harvested with TrypLE™ Express. MKN45 cells (at a cell density of 5×10^6 cells per mL) were dispersed in Alg or Alg-HA_{Mw} solution and extruded as described above (*i.e.* 47 μL per sphere volume). The spheres with the cells were further embedded in an Alg disc (70 μL shell disc) containing bmMSCs (2×10^6 cells per mL) that were previously encapsulated during processing and expanded in αMEM for 3 days. The core–shell system was incubated for 10 days in the presence of αMEM or with bmMSC-conditioned media (CM) obtained from the expansion of stem cells for 3 days (1 : 1 ratio of CM : fresh αMEM).

Cellular viability, morphology and distribution. To evaluate the cellular viability after 10 days of culture, the cells were stained with calcein-AM (1 μg mL^{-1} – green staining, live cells) and propidium iodide (1 μL mL^{-1} – red staining, dead cells). To assess the cellular distribution and expression of the specific cellular markers for MKN45 and for bmMSCs (*i.e.* CD44 and CD90, respectively), the hydrogels were washed with TBS-$CaCl_2$ and fixed with 16% formaldehyde (Pierce™, P1304MP) for at least 1 h at room temperature under shaking. After washing with TBS-$CaCl_2$, the cells were permeabilized with 0.1% Triton X-100 in TBS-$CaCl_2$ for 15 min under stirring, and blocked with 3% BSA in TBS-$CaCl_2$ for 1 h at room temperature. The CD44 and CD90 expression was evaluated using the CD44 monoclonal antibody (1 : 350 in 1% w/v BSA/TBS-$CaCl_2$), followed by rabbit anti-mouse Alexa Fluor-594 (1 : 500 in 1% w/v BSA/TBS-$CaCl_2$) and CD90-FITC (1 : 250 in 1% w/v BSA/TBS-$CaCl_2$), respectively. Nuclei were counterstained with DAPI (1 mg mL^{-1} in 1% BSA in TBS-$CaCl_2$). After 1 h of incubation with the antibodies, the gels were washed with TBS-$CaCl_2$ and observed under a confocal laser scanning microscope (TCS SP8, Leica, Germany).

Cancer cell metabolic activity. The MKN45 viability on a coculture hydrogel was determined using the Cell Titer 96® Aqueous One Solution Cell Proliferation Assay (Promega, USA) as described elsewhere.[25] The MKN45 cell proliferation was analysed using the total amount of double-stranded DNA after 10 days of culture. The core hydrogel was collected and placed in 1 mL of ultrapure water and frozen at −80 °C, for thermal shock. The supernatant was used for DNA quantification using a Quant-iT PicoGreen® dsDNA Assay Kit (Invitrogen, Molecular Probes, Oregon, USA), according to the manufacturer's instructions.

Immunoblotting. Cell lysates were obtained from the MKN45 cells extracted from the spheres of the core–shell hydrogels. The total protein was extracted with radioimmunoprecipitation assay using RIPA buffer (150 mM sodium chloride; 1% Triton-X100; 0.5% sodium deoxycholate; 0.1% sodium

dodecyl sulphate; 50 mM Tris-Base – pH = 8) supplemented with 1× protease (cOmplete™ ROCHE, Sigma-Aldrich, Portugal) and 1× phosphatase (PhosSTOP™ ROCHE, Sigma-Aldrich, Portugal) inhibitor cocktails. Briefly, the spheres were carefully removed from the core–shell hydrogels and washed with cold TBS-$CaCl_2$. The protein lysates were extracted in RIPA buffer for 30 min with 5 min intervals of vortexing. The extracts were centrifuged (18 000*g*, 16 min, 4 °C), and the supernatant was further analysed by western blotting (WB). Each protein, under Laemmli buffer, was denatured at 37 °C for 1 h 30 min and at 95 °C for 5 min prior to use. The lysates, containing 20 μg of protein, were dissolved using 4–12% Bis-Tris Protein Gels (Invitrogen NuPAGE, Thermo Fisher Scientific, USA) and transferred to nitrocellulose membranes (Thermo Fischer Scientific, USA). The membranes were incubated in 4% (m/v) BSA in Tris-buffered saline-Tween (TBS-T, Cell Signalling Technology) and probed with α-smooth muscle actin (1 : 5000), Vimentin (1 : 1000) and E-cadherin (1 : 5000) antibodies. After 3 cycles of 5 min washing with TBS-T, the membranes were incubated with IRDye®800CW anti-Rabbit or anti-Mouse (1 : 10 000) for 1 h and imaged on an Odyssey Infrared Imaging System (LI-COR Biosciences, USA).

ELISA. The expression of IL-6 in the culture medium after 10 days of culture was evaluated by ELISA. The core–shell hydrogels containing MKN45-bmMSCs and the monoculture of MKN45 were incubated in αMEM containing 10% FBS and 1% antibiotic. After 10 days of culture, the medium was collected and analysed using an IL-6 ELISA kit (R&D Systems Inc., Minneapolis, MN, USA), according to the manufacturer's instructions.

Mechanical properties. The cores of the hydrogels were analysed by Atomic Force Microscopy (AFM) using a JPK NanoWizard 3 (JPK, Germany). The stiffness of Alg and Alg-HAM_w spheres was measured in TBS buffer, under QI Advanced Mode using qp-BioAC-CB1 probes (resonance frequency between 65 and 115 kHz; spring constant between 0.15 and 0.55 N m^{-1}; NanoSensors, Germany). Prior to the experiments, the probes were calibrated using the JPK non-contact method. The Young's modulus was calculated from fitting of the approach curves with the Hertz/Sneddon model, using a cone tip shape.

Image analysis. The volume (V) of the clusters was calculated from the confocal laser scanning microscopy images, by measuring the radius (r) of the cellular agglomerates according to the eqn (1) and (2):

$$r = \frac{1}{2}V(\mathrm{d1} \times \mathrm{d2}) \quad (1)$$

$$V = \frac{4}{3}\pi \times r^3 \quad (2)$$

where d1 and d2 are the length and width of the cells' clusters, respectively.

The quantification of fluorescence from the confocal images and densitometric analysis of the WB membranes were performed using ImageJ software (Version 2.0.0-rc-34/1.50a).

Statistical analysis. The normality of the data was analysed using the Shapiro–Wilk test ($p < 0.05$). For the data that did not follow a normal distribution, the Kruskal–Wallis test followed by the Mann–Whitney test was used.

Results and discussion

Development of a core–shell 3D hydrogel

Mimicking the TME is challenging due to its complexity.[13] Cell spheroids and 3D scaffolds are the current *in vitro* TME models used in cancer studies. Whereas spheroids are based on clustering of one (*e.g.* CCs) or more cell types (*e.g.* cancer-associated fibroblasts (CAFs) and MSCs), they lack the dynamic crosstalk between CCs and the surrounding environment;[26] the 3D hydrogel models mimic the features of the extracellular matrix (ECM) composition by using specific components of the ECM, with controlled porosity and mechanical properties.[27]

Here, we developed a core–shell 3D cancer model that resembles the complexity of the TME, combining (1) the presence of HA of different M_ws in the ECM of the cancer tissue; (2) its influence on the behaviour of gastric CCs (*i.e.* MKN45) at the cancer site and of healthy bone marrow (bm) MSCs in the neighbouring regions; and (3) the interplay among HA, CCs and healthy bmMSCs (Fig. 1A).

The proposed system is composed of a core hydrogel's microparticle that contains HA of different M_ws, blended with the biocompatible Alg to generate the 3D polymer network cross-linked under mild conditions, *i.e.* with Ca^{2+}.[28] We performed an initial assessment of the stability of this system and its ability to maintain the HA in the core of the 3D hydrogel. This was executed using labelled HA (*i.e.* HA-FITC) making possible to confirm its incorporation into the core of the construct (Fig. 1B) by fluorescence microscopy.

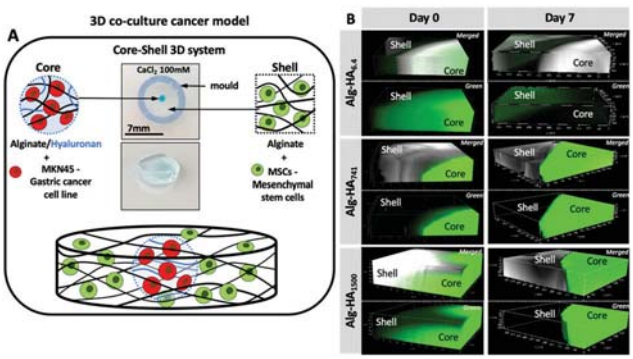

Fig. 1 (A) Graphical illustration of the developed 3D core–shell system used for the co-culture of cancer MKN45 cells and bone marrow mesenchymal stem cells (bmMSCs). Hydrogel images are shown in Fig. S1.† (B) Confocal microscopy images showing the diffusion of the HA (green) from the core to the shell (bottom images, where green corresponds to HA-FITC incorporated in the Alg core; top images merged channels from the transmitted and fluorescence images of the Alg/HA-FITC).

As expected, short HA (*i.e.* 6.4 kDa) is more diffusive: fluorescence can be seen beyond the core of the system even at very short immersion times. This diffusion can explain the similarity between the mechanical properties and stability of Alg and Alg-$HA_{6.4}$ cores (Fig. 2A). However, in general, we observe a reduction of stiffness when HA is combined with Alg, with a higher impact as the HA's M_w increases. HA contributes differently to the stability of the hydrogels, with a clear distinction between shorter HA chains (*i.e.* $HA_{6.4}$) and longer HA chains (*i.e.* HA_{741} and HA_{1500}). Our results are consistent with the ability of the longer chains of HA to partially block the ionic crosslinking of Alg, leading to the formation of hydrogels of lower stiffness (Fig. 2B2). In contrast, the shorter chains of $HA_{6.4}$ are not able to significantly block the activity of the Ca^{2+} ions, presenting a limited impact on the Alg cross-linking (Fig. 2B1).[29,30] Another important point to consider is the very high viscosity of HA_{1500} that strengthens the Alg matrix, partially reverting the loss of stiffness observed for the core composed of Alg-HA_{741}.

After 7 days of immersion (5% CO_2 incubator at 37 °C in cell culture medium, but in the absence of cells), the Alg and Alg-$HA_{6.4}$ spheres lose their integrity due to the release of Ca^{2+} (*i.e.* the Alg crosslinking agent) from the hydrogel network, resulting in the disruption of the Alg matrix.[31]

Longer HA chains (*i.e.* 741 and 1500 kDa) remained within the core even after 7 days of immersion (Fig. 1B) due to the interpenetrating network formed by Alg and the lower mobility and diffusion of the HA of high M_w compared with those of the low M_w polymer. Overall, the generated Alg-HA_{741} and Alg-HA_{1500} networks had lower stiffness values as compared to Alg (Fig. 2A); however they were more stable after 7 days of immersion. In fact, their mechanical properties did not change significantly over time, while the Alg and Alg-$HA_{6.4}$ disassembled during the same time period.

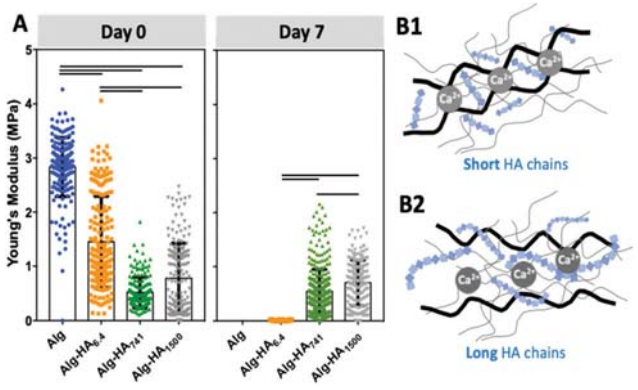

Fig. 2 (A) Mechanical properties of the constructs' cores incorporating HA with different M_ws (*i.e.* 6.4, 741 and 1500 kDa) as a function of immersion time. (B) Schematic presentation of the molecular structure of the cores made from Alg (black) and (B1) short or (B2) long HA chains (blue) that results in the formation of an interpenetrating network. Statistical differences are marked for $p < 0.001$.

The incorporation of MKN45 cells influences the mechanical properties and stability of the hydrogels' core

The stiffness of 3D matrices affects the cellular adhesion and proliferation.[32–35] In turn, cells also modulate the stiffness of the surrounding environment through the secretion of different proteins: the higher deposition of the ECM components in the TME usually leads to a stiffening of the cancer site.[36]

Indeed, we observed that the MKN45 cells encapsulated in the construct's core affected its mechanical properties (Fig. 3). The MKN45 cells formed aggregates with increased cell viability in the presence of HA (Fig. 4A – core). This result can be explained with the recognition of HA by the MKN45 cells.[37] Indeed, confocal microscopy showed a scattered fluorescence signal indicating HA reorganization in the presence of cells (Fig. 3A). At day 0, this change is visible only for the short and diffusive $HA_{6.4}$, *i.e.* immediately after cell encapsulation. However, after 1 day of culture, similar redistribution is also visible for the longer HA_{741} and HA_{1500}. In these cases (especially for HA_{1500}), a blurred fluorescence co-exists with the scattered signal suggesting the role of HA in two processes: interpenetrating network formation (blurred fluorescence) and cell–HA interactions.

Cellular encapsulation reduced the stiffness of the hydrogels (Fig. 2A *vs.* Fig. 3B, at day 0) but the dependence on the HA size was similar to the one obtained for the hydrogels without cells. The main difference was observed after 7 days of culture: the MKN45 cells significantly improved the stability of the Alg and Alg-$HA_{6.4}$ hydrogels. These results are consistent with the ability of the encapsulated cells to proliferate and produce ECM under these experimental conditions leading to improved stability of the 3D hydrogel structure over time.[38]

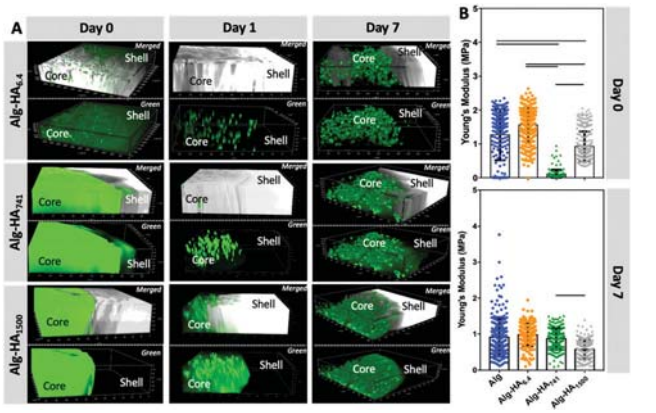

Fig. 3 (A) Confocal microscopy images showing the reorganization of HA (green) by the encapsulated MKN45 cells for different culture times (bottom images, green corresponds to HA-FITC incorporated in the Alg core; top images show the merged channels from the transmitted and fluorescence images of the Alg/HA-FITC). (B) Young's modulus of Alg and Alg-HA_{Mw} hydrogels (core) in the presence of encapsulated MKN45 cells. Statistical differences are marked for $p < 0.001$.

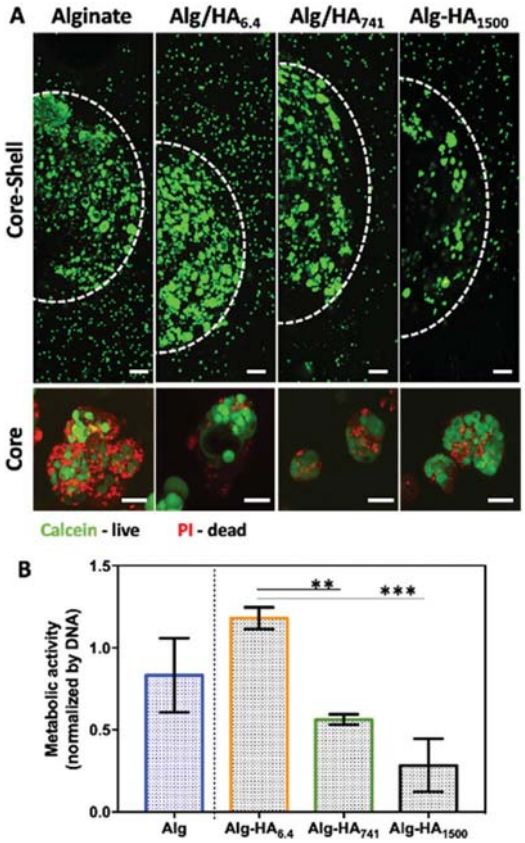

Fig. 4 (A) Live/Dead staining of co-cultures of MKN45 cells (in the core, *i.e.* inside the circle marked by a dashed line) and bmMSCs (in the shell, *i.e.* outside the circle) after 10 days of culture. Scale bars correspond to 200 μm. Lower images correspond to the viability of the MKN45 cells' clusters present inside the core (higher magnification). Scale bars correspond to 50 μm. (B) Metabolic activity of MKN45 cells in the presence of MSCs (core–shell hydrogel). Statistical differences are marked *** for $p < 0.001$ and ** for $p < 0.01$.

The use of Alg to generate the 3D polymer network (through crosslinking with Ca^{2+}) is compatible with cell culture conditions.[37] In addition, Alg also lacks adhesive epitopes and, thus, can serve as a bioinert background that allows the evaluation of the bioactivity of the added HA. Such an approach is advantageous because HA can be immobilized in the 3D construct without any modification. The core containing HA was loaded with CCs (mimicking the cancer site), which were embedded in a hydrogel disc, to which healthy bmMSCs were encapsulated (mimicking the surrounding environment). Moreover, the proposed core–shell model, where CCs are confined in the hydrogel's core, mimic the hypoxic tumor physiological conditions and reduced flow of nutrients.[38] This system was used to evaluate the impact of HA's M_w on cancer invasiveness and the influence of the surrounding healthy cells.

The viability of the cancer (*i.e.* MKN45) and healthy (*i.e.* bmMSCs) cells, cultured on the developed 3D system, was evaluated after 10 days of cell culture. Our Live/Dead staining results show high viability of both cell types in the core and shell of the 3D system (Fig. 4A, S2† – split channels). The formation of MKN45 cell clusters is visible in the core of the hydrogel, with increased cell death in the Alg-only sphere. The addition of HA into the core improves cellular viability, which could be related to the internalization of HA by the MKN45 cells, as suggested by the fluorescence images obtained using HA-FITC (Fig. 3A, days 1 and 7).[37] Moreover, the MKN45 cells seeded on HA of 6.4 kDa present higher metabolic activity when compared to the hydrogels presenting HA of higher M_w, showing the ability of the HA M_w to modulate the proliferation and viability of cells (Fig. 4B).

Cancer cell invasion and protein expression in the presence of mesenchymal stem cells

The influence of MSCs on CC behavior is mediated through the release of pro-inflammatory cytokines and/or growth factors (*e.g.* TGF-beta1, VEGF and IL-6).[39] However, direct MSC-CC contact can also occur and lead to the disruption of CC agglomerates mainly through the cleavage of the cell–cell junctions, which are maintained by E-cadherin.[15,40] The presence of MSCs in the TME also increases the sensitivity of CCs to anti-cancer drugs.[41] The MSC : CC ratio is also critical for any outcome, including changes in CC invasiveness and tumor progression.[18,26]

To mimic the complexity of the TME, we encapsulated MSCs in the shell of the construct, which was designed to be in direct contact with the core (representing the cancer site) containing the encapsulated CCs. To track the movement of each cell type, we tagged cells for the mesenchymal stem cell marker, CD90,[42] and the transmembrane HA receptor, CD44, in all studied cells.[43] Both cell types express CD90 and CD44 (Fig. S3†), but the relative expression is very different and can be used to distinguish MKN45 cells from bmMSCs. Our results show that MKN45 cells (encapsulated in the Alg-$HA_{6.4}$ core) escape into the Alg shell. When the core contained longer HA chains (*i.e.* 741 and 1500 kDa), no MKN45 invasion was observed but bmMSCs migrated from the shell into the core of the construct (Fig. 5A and S4†).

In the TME, the secretion of pro-inflammatory cytokine Interleukin-6 (IL-6) is linked to tumorigenesis, cancer cell proliferation and metastasis.[44] Herein, we observed a significant increase of the IL-6 protein level in the medium from the co-cultures of the core–shell hydrogels containing Alg-$HA_{6.4}$ (Fig. 6). This is in good agreement with the migration pattern of MKN45 cells, which showed an invasive character in the presence of HA of low M_w. The absence of IL-6 expression on MKN45 monoculture (Fig. S7†), as previously observed by others,[45] shows that bmMSCs in the tumour vicinity trigger the aggressive character of the gastric CCs, which may be correlated with poor prognosis of cancer and resistance to chemotherapy.[45]

The invasion of MKN45 cells from the Alg-$HA_{6.4}$ core into the shell was also observed in the absence of bmMSCs (Fig. 5A; monoculture, white arrows) and this can be associated with (1) fast solubilization of the core structure, through

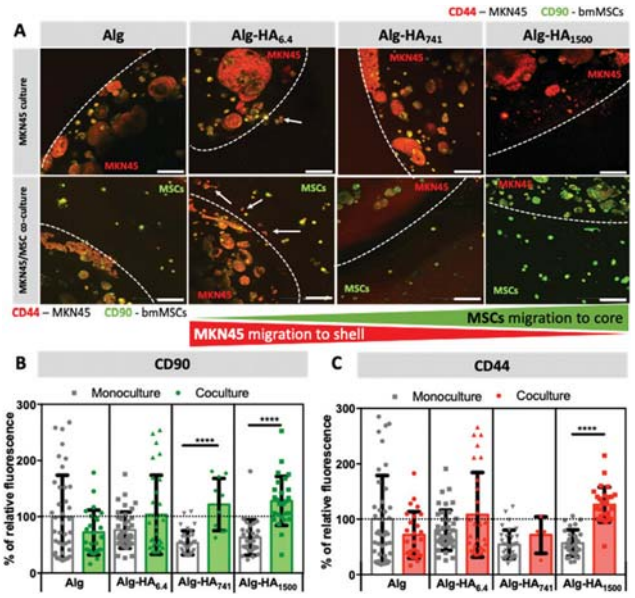

Fig. 5 (A) Invasion of MKN45 cells (mono- and co-culture) into the shell and recruitment of bmMSCs (co-culture) into the core. (B and C) Relative fluorescence intensity (normalised to Alg construct under monoculture conditions) measured for the cells' agglomerates in the core that were immunolabelled for (B) CD90 and (C) CD44. Scale bars correspond to 200 μm. Statistical differences are marked **** for $p < 0.0001$.

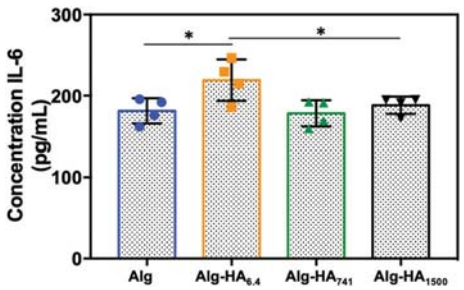

Fig. 6 IL-6 secretion measured by ELISA from the cells seeded in the hydrogels under co-culture conditions. Statistical differences are marked * for $p < 0.05$.

the release of Ca^{2+} cations (as previously shown in Fig. 1 and 2), which leads to the reorganization of the core matrix increasing the invasion of MKN45 cells; (2) the HA gradient generated upon the diffusion of HA into the shell (Fig. 1B) acting as directional cues for CC migration; and (3) the internalization of $HA_{6.4}$ by CCs, as suggested by the fluorescence images of HA-FITC on the CC sites (core, Fig. 3A) which could act as a signaling mechanism to induce CCs' invasion.[38,46] bmMSCs cultured alone did not migrate from the shell to the HA-rich core (Fig. S4†); however, in the presence of MKN45 cells, it appears that the stem cells colonized Alg-HA_{1500} (Fig. 5A). The observed result (high relative intensity of green in the core, Fig. 5A and B) can be also due to increased CD90 expression by MKN45 in the presence of bmMSCs in the vicinity of the CCs. The same variation of CD90 expression was observed for the MKN45 cell cultures supplemented with medium from bmMSC expansion (Fig. S6†). This result showed that MSC-secretome alone is able to modulate MKN45 behavior but the direct MSC–MKN45 contact amplifies this response.

Disruption of MKN45 cell–cell contacts in the presence of MSCs

The ability of bmMSCs to modulate the cell-to-cell contact in tumors was assessed from the capacity of MKN45 cells to form aggregates when cultured alone or together with bmMSCs (Fig. 7). We observed significantly smaller MKN45 aggregates in Alg and Alg-HA_{1500} in the presence of bmMSCs (Fig. 7B). We believe that the co-culture on an Alg-only system induces a faster degradation of the hydrogel, compromising cellular adhesion and proliferation. On the other hand, bmMSCs cultured in the shell of the Alg-HA_{1500} rich-core system promote the formation of smaller CC aggregates and therefore inhibit tumor growth. In fact, it has been previously reported that the

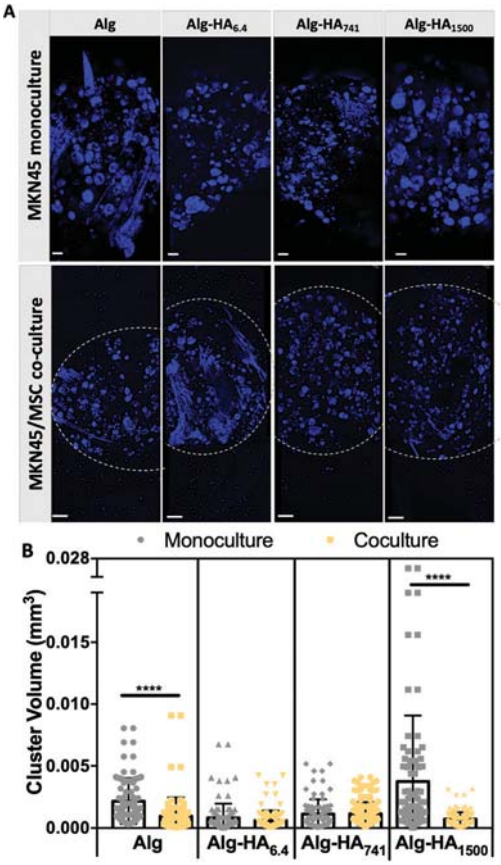

Fig. 7 Influence of the bmMSCs (cultured in the shells of the hydrogels) on the aggregation of MKN45 cells in the core of the construct: (A) confocal microscopy images of MKN45 cells cultured alone (monoculture) and together with bmMSCs (co-culture) and immunostained with DAPI (cell nuclei). (B) Volume analysis of the CCs' aggregates generated under different cell culture conditions. Scale bars correspond to 200 μm. Statistical differences are marked **** for $p < 0.0001$.

same tumor inhibition occurred when a small, but relevant, number of MSCs (a CC : MSCs ratio of 2 : 1) were injected into the tumor site.[47]

The mesenchymal/epithelial markers expressed by the MKN45 cells encapsulated in the core of the construct was evaluated by western blotting (WB, Fig. 8). Under co-culture conditions, the cells in the core enhance the expression of vimentin, a mesenchymal marker[42] for the Alg, Alg-HA_{741} and Alg-HA_{1500} hydrogels' cores. It is noteworthy that vimentin was not expressed by MKN45 cells cultured alone or supplemented with bmMSC-conditioned media (Fig. S8†). This observation is consistent with the idea that either vimentin is derived from the epithelial to mesenchymal transition of the MKN45 cells or the bmMSCs attracted to the core are the source of this vimentin expression. Overall, our results are consistent with the latter possibility as bmMSCs are observed in the core of the hydrogel formulated with HA of higher M_w (Fig. 5A). Moreover, the presence of HA of high M_w has been reported to induce CCs to produce chemotactic factors, such as cytokines and growth factors, which act as chemoattractants for MSCs, further supporting our results that show the recruitment of bmMSCs to the core of the 3D system.[48–50]

For the same samples (*i.e.* Alg, Alg-HA_{741} and Alg-HA_{1500}) we also observed overexpression of E-cadherin by the cells in the core of the 3D system showing an increment of the cell–cell contacts. This result indicates the promotion of the epithelial transition of MKN45 cells when they are in contact with bmMSCs. The absence of vimentin expression and a downregulation of E-cadherin (responsible for the epithelial cell–cell junctions) in the MKN45 cells encapsulated in the Alg-$HA_{6.4}$ core suggest that the CCs are not in direct contact with MSCs in the core of the hydrogel, but instead CC invasion into the shell is induced (loss of E-cadherin expression), as previously reported.[51]

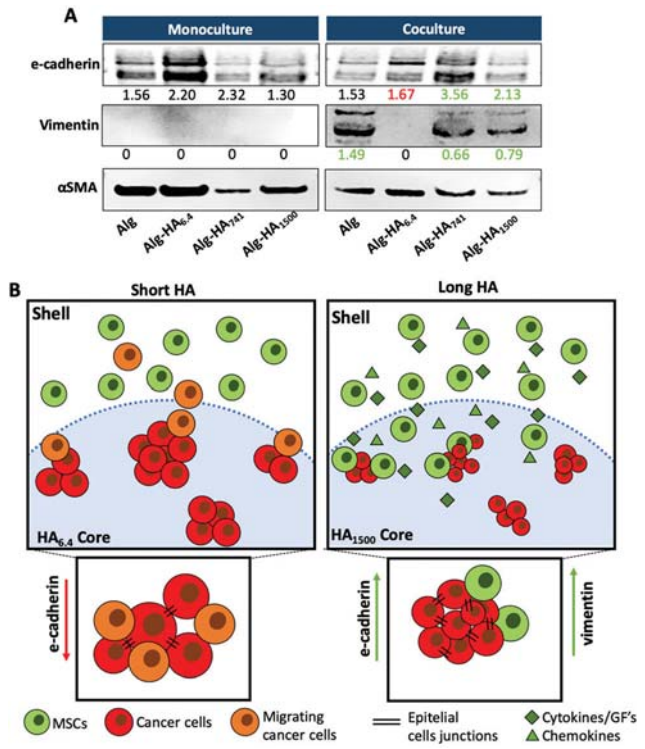

Fig. 8 (A) Western blot analysis of E-cadherin (120 kDa), vimentin (55 kDa) and smooth muscle actin (αSMA – 40 kDa) as the loading control, from the cells' protein lysates present in the core of the hydrogel. The values represent the densitometric intensity normalized to αSMA. (B) Graphical presentation of the effect of the HA size on the cellular response of MKN45 (red) cells and bmMSCs (green).

Conclusions

We developed a 3D core–shell model that is able to recapitulate a series of mechanical, biochemical and biological features of a gastric TME. Using co-culturing conditions (MKN45 cells at the tumour site and bmMSCs in its periphery) we were able to mimic the influence of healthy bmMSCs on the CCs' behavior. We further demonstrate that the HA's M_w at the cancer site is able to modulate CCs' behavior. Low M_w HA, *e.g.* $HA_{6.4}$, induces a migratory phenotype in MKN45 cells, which also internalize HA immediately after cell seeding. In contrast, HA of high M_w, *e.g.* HA_{1500}, does not promote an invasive behavior on MKN45 CCs; instead, it attracts bmMSCs to the cancer site, reducing the growth of CC clusters. Overall, with the developed core–shell 3D model, we were able to mimic the TME and assess the influence of the biochemical features of specific components of the cancer ECM, *e.g.* HA and its M_w, as well as the presence of bmMSCs, on CCs' behaviour.

Additional statement

All experiments were performed in accordance with the Guidelines of the Code of Ethical Conduct of the University of Minho and Experiments were approved by the Ethics Committee of Hospital da Prelada (Ref. DC 05/2015). Informed consent was obtained from the human participants in this study.

Conflicts of interest

There are no conflicts to declare.

Acknowledgements

We acknowledge the financial support from the European Commission and the Horizon 2020 – WIDESPREAD programme, under the grant agreement number #668983-FORECAST. SA acknowledges the Portuguese Foundation for Science and Technology for her PhD grant (SFRH/BD/112075/2015).

References

1 L. L. Hui and Y. Chen, *Cancer Lett.*, 2015, **368**, 7–13.
2 M. Wang, J. Zhao, L. Zhang, F. Wei, Y. Lian, Y. Wu, Z. Gong, S. Zhang, J. Zhou, K. Cao, X. Li, W. Xiong, G. Li, Z. Zeng and C. Guo, *J. Cancer*, 2017, **8**, 761–773.
3 S. S. Pinho and C. A. Reis, *Nat. Rev. Cancer*, 2015, **15**, 540–555.
4 A. V. Taubenberger, L. J. Bray, B. Haller, A. Shaposhnykov, M. Binner, U. Freudenberg, J. Guck and C. Werner, *Acta Biomater.*, 2016, **36**, 73–85.
5 F. A. Venning, L. Wullkopf and J. T. Erler, *Front. Oncol.*, 2015, **5**, 224.
6 S. Mereiter, A. M. Martins, C. Gomes, M. Balmana, J. A. Macedo, K. Polom, F. Roviello, A. Magalhaes and C. A. Reis, *FEBS Lett.*, 2019, **593**, 1675–1689.
7 T. Chanmee, P. Ontong and N. Itano, *Cancer Lett.*, 2016, **375**, 20–30.
8 L. P. Setälä, M. I. Tammi, R. H. Tammi, M. J. Eskelinen, P. K. Lipponen, U. M. Ågren, J. Parkkinen, E. M. Alhava and V. M. Kosma, *Br. J. Cancer*, 1999, **79**, 1133–1138.
9 C. Walker, E. Mojares and A. Del Río Hernández, *Int. J. Mol. Sci.*, 2018, **19**(10), 3028.
10 Z. K. Price, N. A. Lokman and C. Ricciardelli, *Cancers*, 2018, **10**(12), 482.
11 C. Yang, M. Cao, H. Liu, Y. He, J. Xu, Y. Du, Y. Liu, W. Wang, L. Cui, J. Hu and F. Gao, *J. Biol. Chem.*, 2012, **287**, 43094–43107.
12 F. Chen, X. Zhuang, L. Lin, P. Yu, Y. Wang, Y. Shi, G. Hu and Y. Sun, *BMC Med.*, 2015, **13**, 45.
13 H. Sawayama, T. Ishimoto and H. Baba, *J. Cancer Metastasis Treat.*, 2018, **4**, 10.
14 S. Mereiter, M. Balmana, D. Campos, J. Gomes and C. A. Reis, *Cancer Cell*, 2019, **36**, 6–16.
15 A. Dittmer, K. Hohlfeld, J. Lützkendorf, L. P. Müller and J. Dittmer, *Cell. Mol. Life Sci.*, 2009, **66**, 3053–3065.
16 A. Y. Khakoo, S. Pati, S. A. Anderson, W. Reid, M. F. Elshal, I. I. Rovira, A. T. Nguyen, D. Malide, C. A. Combs, G. Hall, J. Zhang, M. Raffeld, T. B. Rogers, W. Stetler-Stevenson, J. A. Frank, M. Reitz and T. Finkel, *J. Exp. Med.*, 2006, **203**, 1235–1247.
17 W. Zhu, M. Wang, Y. Fu, N. J. Castro, S. W. Fu and L. G. Zhang, *Acta Biomater.*, 2015, **14**, 164–174.
18 B. L. Yen and M.-L. Yen, *J. Cancer Mol.*, 2008, **4**(1), 5–9.
19 F. Djouad, C. Bony, F. Apparailly, P. Louis-Plence, C. Jorgensen and D. Noel, *Transplantation*, 2006, **82**, 1060–1066.
20 A. H. Klopp, L. Lacerda, A. Gupta, B. G. Debeb, T. Solley, L. Li, E. Spaeth, W. Xu, X. Zhang, M. T. Lewis, J. M. Reuben, S. Krishnamurthy, M. Ferrari, R. Gaspar, T. A. Buchholz, M. Cristofanilli, F. Marini, M. Andreeff and W. A. Woodward, *PLoS One*, 2010, **5**, e12180.
21 I. W. Mak, N. Evaniew and M. Ghert, *Am. J. Transl. Res.*, 2014, **6**, 114–118.
22 S. Melissaridou, E. Wiechec, M. Magan, M. V. Jain, M. K. Chung, L. Farnebo and K. Roberg, *Cancer Cell Int.*, 2019, **19**, 16.
23 D. S. Ferreira, A. P. Marques, R. L. Reis and H. S. Azevedo, *Biomater. Sci.*, 2013, **1**, 952–964.
24 D. S. da Costa, R. A. Pires, A. M. Frias, R. L. Reis and I. Pashkuleva, *J. Mater. Chem.*, 2012, **22**, 7172–7178.
25 S. Amorim, A. Martins, N. M. Neves, R. L. Reis and R. A. Pires, *J. Mater. Chem. B*, 2014, **2**, 6939–6946.
26 L. P. Ferreira, V. M. Gaspar and J. F. Mano, *Biomaterials*, 2018, **185**, 155–173.
27 G. Rijal and W. Li, *Sci. Adv.*, 2017, **3**, e1700764.
28 F. Hached, C. Vinatier, P. G. Pinta, P. Hulin, C. Le Visage, P. Weiss, J. Guicheux, A. Billon-Chabaud and G. Grimandi, *Stem Cells Int.*, 2017, **2017**, 9303598.
29 M. J. Costa, A. M. Marques, L. M. Pastrana, J. A. Teixeira, S. M. Sillankorva and M. A. Cerqueira, *Food Hydrocolloids*, 2018, **81**, 442–448.
30 I. Braccini and S. Perez, *Biomacromolecules*, 2001, **2**, 1089–1096.
31 G. Chan and D. J. Mooney, *Acta Biomater.*, 2013, **9**, 9281–9291.
32 H. N. Kim and N. Choi, *BioChip J.*, 2019, **13**, 8–19.
33 M. Cavo, M. Fato, L. Peñuela, F. Beltrame, R. Raiteri and S. Scaglione, *Sci. Rep.*, 2016, **6**, 35367.
34 J. E. Kim, D. S. Reynolds, M. H. Zaman and M. Mak, *Integr. Biol.*, 2018, **10**, 232–241.
35 C. Liu, Y. Liu, X. X. Xu, H. Wu, H. G. Xie, L. Chen, T. Lu, L. Yang, X. Guo, G. W. Sun, W. Wang, X. J. Ma and X. He, *Exp. Cell Res.*, 2015, **330**, 123–134.
36 H. Yu, J. K. Mouw and V. M. Weaver, *Trends Cell Biol.*, 2011, **21**, 47–56.
37 A. Canibano-Hernandez, L. Saenz Del Burgo, A. Espona-Noguera, G. Orive, R. M. Hernandez, J. Ciriza and J. L. Pedraz, *Mol. Pharm.*, 2017, **14**, 2390–2399.
38 M. J. Kratochvil, A. J. Seymour, T. L. Li, S. P. Paşca, C. J. Kuo and S. C. Heilshorn, *Nat. Rev. Mater.*, 2019, **4**, 606–622.
39 S. M. Ridge, F. J. Sullivan and S. A. Glynn, *Mol. Cancer*, 2017, **16**, 31.
40 L. P. Ferreira, V. M. Gaspar, R. Henrique, C. Jeronimo and J. F. Mano, *Biotechnol. J.*, 2017, **12**, 12.
41 A. Dittmer, A. Fuchs, I. Oerlecke, B. Leyh, S. Kaiser, J. W. Martens, J. Lutzkendorf, L. Muller and J. Dittmer, *Int. J. Oncol.*, 2011, **39**, 689–696.
42 R. Secunda, R. Vennila, A. M. Mohanashankar, M. Rajasundari, S. Jeswanth and R. Surendran, *Cytotechnology*, 2015, **67**, 793–807.
43 S. Amorim, D. S. da Costa, D. Freitas, C. A. Reis, R. L. Reis, I. Pashkuleva and R. A. Pires, *Sci. Rep.*, 2018, **8**, 16058.
44 D. T. Fisher, M. M. Appenheimer and S. S. Evans, *Semin. Immunol.*, 2014, **26**, 38–47.
45 I. H. Ham, H. J. Oh, H. Jin, C. A. Bae, S. M. Jeon, K. S. Choi, S. Y. Son, S. U. Han, R. A. Brekken, D. Lee and H. Hur, *Mol. Cancer*, 2019, **18**, 68.
46 R. Stern, A. A. Asari and K. N. Sugahara, *Eur. J. Cell Biol.*, 2006, **85**, 699–715.

47 F. Djouad, C. Bony, F. Apparailly, P. Louis-Plence, C. Jorgensen and D. Noël, *Transplantation*, 2006, **82**, 1060–1066.
48 H. Y. Lee and I. S. Hong, *Cancer Sci.*, 2017, **108**, 1939–1946.
49 E. Spaeth, A. Klopp, J. Dembinski, M. Andreeff and F. Marini, *Gene Ther.*, 2008, **15**, 730–738.
50 Y. Rattigan, J.-M. Hsu, P. J. Mishra, J. Glod and D. Banerjee, *Exp. Cell Res.*, 2010, **316**, 3417–3424.
51 Y. F. Zhao, S. P. Qiao, S. L. Shi, L. F. Yao, X. L. Hou, C. F. Li, F. H. Lin, K. Guo, A. Acharya, X. B. Chen, Y. Nie and W. M. Tian, *ACS Appl. Mater. Interfaces*, 2017, **9**, 9327–9338.